Composite Structures 351 (2025) 118610

Contents lists available at ScienceDirect

Composite Structures

journal homepage: www.elsevier.com/locate/compstruct

Examining infrared thermography based approaches to rapid fatigue characterization of additively manufactured compression molded short fiber thermoplastic composites

P. Pathak [a], S. Gururaja [a,*], V. Kumar [c], D. Nuttall [c], A. Mahmoudi [b], M.M. Khonsari [b], U. Vaidya [c,d]

[a] Department of Aerospace Engineering, Auburn University, Auburn, AL, USA
[b] Department of Mechanical Engineering, Louisiana State University, Baton Rouge, LA, USA
[c] Manufacturing Science Division, Oakridge National Lab, Oak Ridge, TN, USA
[d] Tickle College of Engineering, University of Tennessee, Knoxville, TN, USA

ARTICLE INFO

Keywords:
SFTs
AM-CM
Infrared thermography
Fatigue
Self-heating

ABSTRACT

A novel additive manufacturing (AM) methodology combined with a compression molding (CM) process has been previously developed to optimize the microstructure of short fiber thermoplastic (SFTs) composites with higher fiber alignment and lower porosity, yielding superior stiffness, strength, and structural integrity. The current work examines the efficacy of the 'passive' infrared thermography (IRT) techniques for rapid fatigue characterization of SFTs that use the surface temperature evolution during cyclic loading due to self-heating as a fatigue indicator. A comparison of fatigue limits obtained from traditional stress-life (SN) ($\approx 53.1\%\sigma_{uts}$) and IRT ($\approx 54.1\%\sigma_{uts}$) shows a close match. However, the SN curve required 18 specimens and two weeks of continuous cyclic testing, while IRT used three specimens with 5 h of testing. Thus, the IRT approach provides an accelerated testing framework for rapidly estimating the fatigue limit. Additionally, existing phenomenological approaches to IRT fatigue characterization have been examined.

1. Introduction

The usage of fiber-reinforced polymer (FRP) structural composite is expected to increase steadily for the coming decade, spurred by aerospace, marine, and automotive applications for improved lightweight and structural performance [1–4]. Within this domain, short fiber reinforced thermoplastic composites (SFTs) with carbon fibers are increasingly favored in the industry due to their mechanical advantages, including enhanced fatigue resistance, improved strength, and ease of production [5]. However, due to material flow dynamics, chopped fibers in SFTs have variable fiber orientations, affecting these materials' mechanical and thermal performance [6,7]. In response to this challenge, Oakridge National Lab (ORNL) has recently developed additively manufactured compression molding (AM-CM) technique that integrates the AM process ensuring excellent fiber orientational control and lower porosity due to the CM process [1,8–11]. Multiple efforts are underway to incorporate AM-CM components into various applications, particularly in automotive components that are fatigue critical. Investigating the high cycle fatigue (HCF) behavior of these novel AM-CM SFTs is a priority for institutions like ORNL and OSHKOSH. For instance, they are collaborating on the development of a concrete truck chute using SFTs via the AM-CM process. This component will be tested for fatigue performance to estimate the service life. Assessing the fatigue performance of SFTs, especially accounting for their microstructural variability (fiber alignment and porosity), remains a challenge due to a multitude of printing parameters that influence the microstructure, such as nozzle diameter, extrusion rate, and printing speed. Therefore, a rapid method to understand the fatigue behavior of AM-CM structures is highly desirable.

Ensuring safety and reliability requires an accurate mechanistic understanding of the material degradation under HCF loading and in-service conditions [12]. Unlike metals, fatigue in composites is multi-modal and multiscale due to inherent material heterogeneity, anisotropy, and hierarchy [13]. SFTs are particularly valued for their mechanical properties, which can be tailored by controlling fiber size, orientation, and the composite's microstructure. The anisotropic nature of these materials significantly influences their tensile strength and elastic modulus due to the directional properties imparted by the fibers. Recent studies [5,14–19] have focused on modeling the elastic and thermoelastic properties of SFTs to predict their behavior under fatigue loading. These models are essential for understanding how SFTs will

* Corresponding author.
E-mail address: suhasini.gururaja@auburn.edu (S. Gururaja).

https://doi.org/10.1016/j.compstruct.2024.118610
Received 19 March 2024; Received in revised form 20 September 2024; Accepted 22 September 2024
Available online 29 September 2024

perform in real-world applications subjected to various environmental and operational stresses [20,21]. Fatigue damage, which accumulates in materials subjected to cyclic loading, can significantly impact the residual stiffness and strength of SFTs. Understanding this damage and its effects on material properties is essential for predicting the life and safety of structures made from SFTs [5,22]. Researchers have developed various experimental methods and empirical models to determine fatigue damage and conducted both static and dynamic tests to ascertain the elastic moduli and strengths of virgin SFTs with various fiber orientations. These studies have also included destructive and non-destructive cyclic tests to identify damage progression and create conventional stress life (SN) curves representing fatigue behavior.

Characterizing the fatigue damage accumulation using traditional techniques is challenging due to the variable properties of SFTs. Furthermore, SN fatigue testing can be resource-intensive and time-consuming [23–25]. Recently, new techniques such as the thermographic and ultrasonic methods have been developed that allow for rapid assessment of fatigue life [26]. IR thermography monitors surface self-heating to determine the critical stress for initiating irreversible fatigue damage. Ultrasonic fatigue testing can rapidly assess fatigue behavior from high-cycle to very high-cycle regimes, also relying on self-heating phenomenon. This use of self-heating to assess the state of damage in the material has received particular attention as a means of rapid fatigue characterization [13,21,27–31]. Under cyclic loading, the dissipated hysteretic energy due to plastic deformation (in metals) or other irreversible thermodynamic dissipative processes is transformed into heat [32–34]. Infrared thermography (IRT) has shown promising results across various stress ratios in prior studies, affirming its effectiveness and suitability for diverse testing conditions [24,25,30,35].Thanks to advancements in IRT, cooled IR cameras are now widely available and affordable, enabling the measurement of these small fluctuations in surface temperatures during fatigue.

The fundamental basis of the IRT approach lies in the correlation between surface temperatures and the inherent damage state of a specimen under cyclic loading [36]. Under constant amplitude fatigue (CAF), three distinct phases can be identified from a specimen's surface temperature plots: a region of rapid temperature rise (Phase I), followed by a cyclic stabilized mean temperature (ΔT_{stab}) corresponding to a steady-state damage progression (Phase II), and a final third region (Phase III) accompanied by unsustainable rapid temperature rise corresponding to final failure (cf. Fig. 1(a)). The Phase II ΔT_{stab} of the specimen increases with increasing stress levels (Fig. 1(b)). When ΔT_{stab} temperatures are plotted to applied stress (σ_{max}), a bi-linear curve that defines the HCF strength (HCFS) is obtained (Fig. 1(c)). A step-loading method, where the σ_{max} is increased in steps of constant stress ratio (R) while ensuring that the specimen is in Phase II region, allows for the estimation of HCFS using a single specimen [13,36–38]. Thus, fatigue limits can be rapidly estimated from fewer samples. This approach has been validated with the endurance limit of various FRP systems generated from SN curves [24,37,39–42].

Cyclic loading-induced self-heating is, in effect, a measure of accumulated entropy or material degradation in a material. This fundamental concept has been formalized using the concept of fatigue fracture entropy (FFE) as a material property [16,27,34,35,43–46]. Recently, by plotting initial temperature rise ($\frac{dT}{dt}|_{t=0} = R_\theta$) (see Fig. 1(a)) at various σ_{max} for CAF, a novel method of determining HCFS limit has been demonstrated for metals [44]. Meneghetti [13] observed that the cooling rate (R_c) associated with interrupting a cyclic fatigue test once the material's surface temperature has reached a stable value, ΔT_{stab}, is indicative of thermal power loss per unit volume of the material, which is a more fundamental parameter indicative of the material's fatigue damage state (cf. Fig. 1(a)). Using R_c or R_θ would potentially enable the determination of HCFS without needing a pristine specimen at each load level under CAF. Thus, these methods qualify as accelerated fatigue life methods. However, both R_c and R_θ techniques have been derived for homogeneous materials (metals); the applicability of these approaches to heterogeneous composite systems, such as SFTs, has not been extensively examined.

Full-field temporal surface temperature data reveal fatigue damage onset and progression and relate to energy dissipation [25]. The process employs an algorithm to extract pixel-by-pixel specimen's surface temperature data to evaluate the temperature signal amplitude, phase of the thermoelastic signal, and the amplitude of the second Fourier harmonic component associated with intrinsic dissipation [29,36,38] as shown in Eq. (1).

$$S_m(t) = (S_0 + at) + S_1 \sin(\omega t + \phi) + S_2 \sin(2\omega t) \tag{1}$$

S_m is the thermal signal (not radiometrically calibrated) in the time (t) domain. In this equation, $(S_0 + at)$ represents the increase in mean temperature, inclusive of ambient temperature effects, during cyclic mechanical loading in terms of radiometric signal, ω is the angular frequency of the mechanically imposed cyclic load, ϕ is the phase shift of the first harmonic component, S_1 and S_2 are related to the amplitude of the first harmonic component and the second Fourier harmonic component, respectively. Here, S_1 corresponds to signal variation related to the thermoelastic effect, while S_2 is proportional to the amplitude of intrinsic dissipation [47].

IRT is often used in conjunction with tools such as extensometers [48], laminography [49], acoustic emission [50], laser vibrometry [51], and digital image correlation (DIC) [52] to identify static and fatigue damage in composite materials [37,53]. These tools provide volumetric damage information that complements the surface damage information provided by an IR camera. Stiffness degradation during cyclic loading quantifies damage evolution in composite specimens that are given by Eq. (2) [12,18,21,32,54–58]:

$$D(N) = 1 - \frac{E_N}{E_0} \tag{2}$$

Here, $D(N)$ symbolizes damage accumulation after the Nth loading cycle, E_N represents the specimen's stiffness after the Nth cycle, and E_0 is the initial stiffness. As the stress level or number of cycles increases, the damage ($D(N)$) and the temperature difference (ΔT) also increase. Thus, measuring the temperature (T) provides valuable insight into the extent of damage (D) [37,39,42,48].

Although the application of IRT for rapid fatigue limit estimation for continuous FRPs or randomly distributed SFTs has been explored [17,29,30,32,35,37,39,59], its adaptability to novel AM-CM SFTs has not been assessed. In the current work, the applicability of IRT to rapidly estimate the fatigue limit of AM-CM SFTs has been investigated. The interrelationships between thermal dissipation measured via surface temperatures and volumetric stiffness degradation under tensile cyclic loading for 20 wt% chopped carbon fiber (CF)/acrylonitrile butadiene styrene (ABS) SFTs manufactured via AM-CM have been assessed. The applicability of the established phenomenological rapid fatigue limit assessment, namely, ΔT_{stab} vs. σ_{max}, R_θ, R_c, and S_2, has been examined. In addition, the present study compares the temperature-based IRT methods used to assess rapid fatigue limits with data obtained from the traditional SN approach.

2. Materials and methods

2.1. Materials

Fig. 2(a) presents an overview of AM-CM process at ORNL. Starting with 20 wt% CF/ABS pellets melted in an extruder, the material is deposited through a robotic arm at a 1200 rpm motor speed, nozzle speed of 280 mm/s, and a 9.88 mm gap between the substrate and the nozzle outlet (see Fig. 2(a)). The nozzle, with a diameter of 7.62 mm, operates at a temperature of 423 K during the extrusion process. Upon completion of the AM process, the substrate was compressed and molded by applying a pressure of 500 kN for 5 min to minimize process-induced porosity. The entire additive manufacturing followed by compression

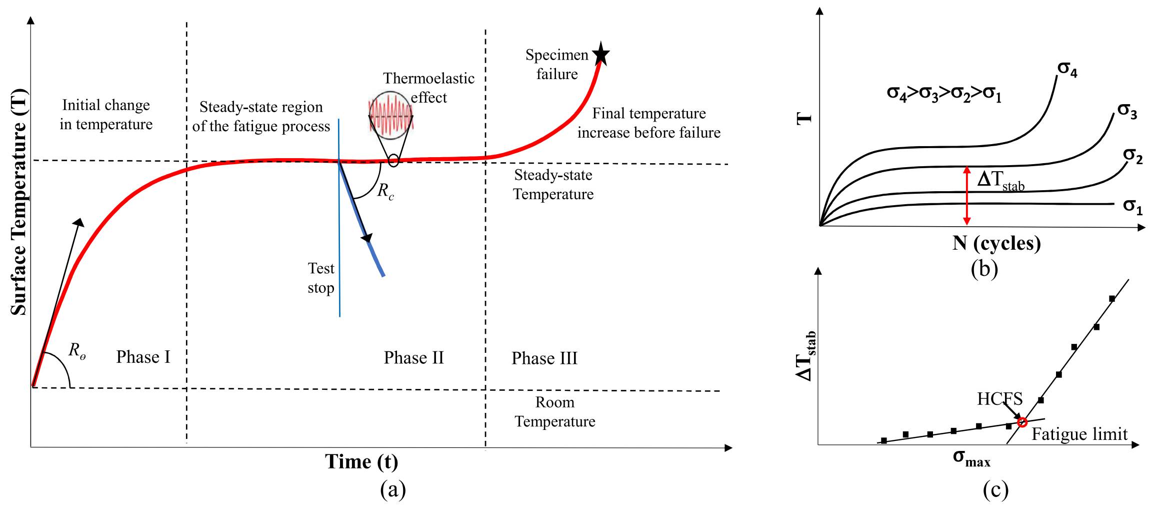

Fig. 1. (a) Typical surface temperature evolution with time under constant amplitude fatigue loading, (b) ΔT_{stab} for increasing applied CAF stress(σ) values, and (c) Estimation of HCFS from the bilinear fitting of the ΔT_{stab} versus σ_{max} curve [16,37,42].

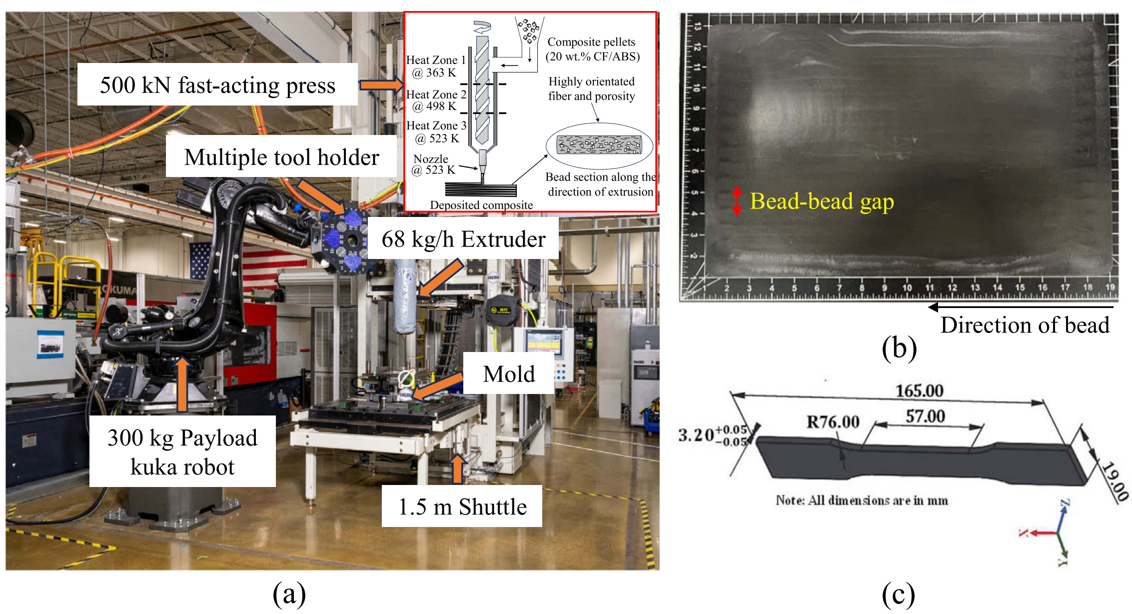

Fig. 2. (a) Robotic arm and fast acting press used in the AM-CM process at ORNL, (b) A CF/ABS composite panel produced via AM-CM process highlighting the bead directions due to additive manufacturing distinguishable bead patterns, and (c) ASTM D638 Type I specimen dimensions used for waterjet cutting and subsequent quasi-static and fatigue testing. All specimens have been machined along the bead direction.

molding takes 15 min, resulting in flat composite panels measuring approximately 450 mm × 300 mm × 3.5 mm in thickness (see Fig. 2(b)).

The AM-CM process induces a distinctive microstructure, where chopped fibers align along the bead direction, leading to directionally dependent properties. In this study, all specimens are machined along this preferentially fiber-aligned direction using abrasive waterjet machining, adhering to ASTM D638 Type I recommended specimen dimensions (see Fig. 2(c)) [60]. The choice of ASTM D638 Type I was based on existing literature [60] for reinforced composites and the thickness of the laminates, which ranged from 4 to 6 mm [61,62]. Prior to mechanical testing (static and fatigue), it was ensured that the specimen surfaces were within the required tolerance limits per ASTM D638 Type I specifications [60].

2.2. Microstructural characterization

To determine the fiber orientation distributions (FODs) and the fiber length distributions (FLDs), X-ray micro-computed tomography (xCT) was performed on the SFT specimens using the Zeiss Versa 620 XRM, following the detailed steps as explained in these referenced papers [63–65]. Samples, measuring 10 × 10 × 3.2 mm, were extracted from the central region of the fabricated plates, and xCT data were collected at 80 kV and 125 μA source setting with 4x scintillator objective lens and 2x2 binning, resulting in a pixel size of about 1 μm. Subsequently, three-dimensional (3D) tomographic reconstructions were performed with appropriate noise reduction and thresholding to determine FOD/FLDs using Avizo 9.3.0 with the XFiber module from grayscale intensity values. Porosity analysis using DragonflyPRO (Version 3.5) revealed a void content of ≈2% with porosity sizes lower than the fiber diameter (8 μm). Although AM-CM can provide up to 80% fiber alignment in the deposition direction by optimizing the printing parameters, the print parameter used in this work resulted in 60% fiber alignment within the range of 0–30° with a typical length of 50–75 μm in the bead direction (cf. Fig. 3(b) and (c)).

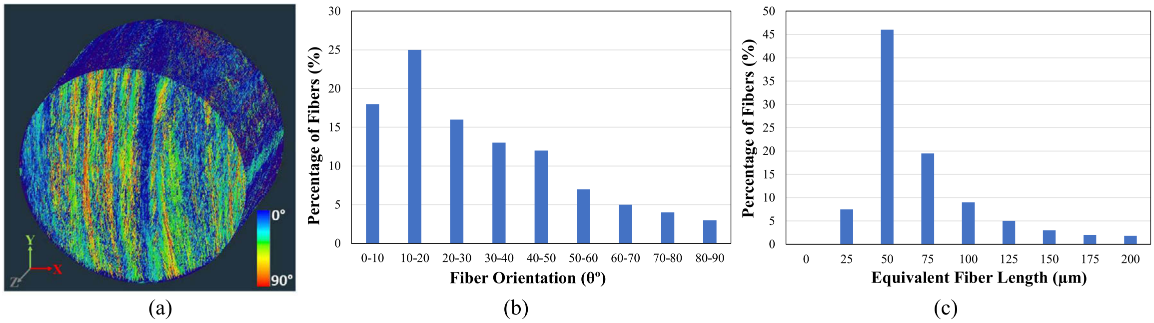

Fig. 3. (a) Microstructure of CF/ABS (xCT) indicating a high degree of fiber alignment, (b) statistical distribution of fiber orientations, and (c) statistical distribution of fiber lengths measured from xCT.

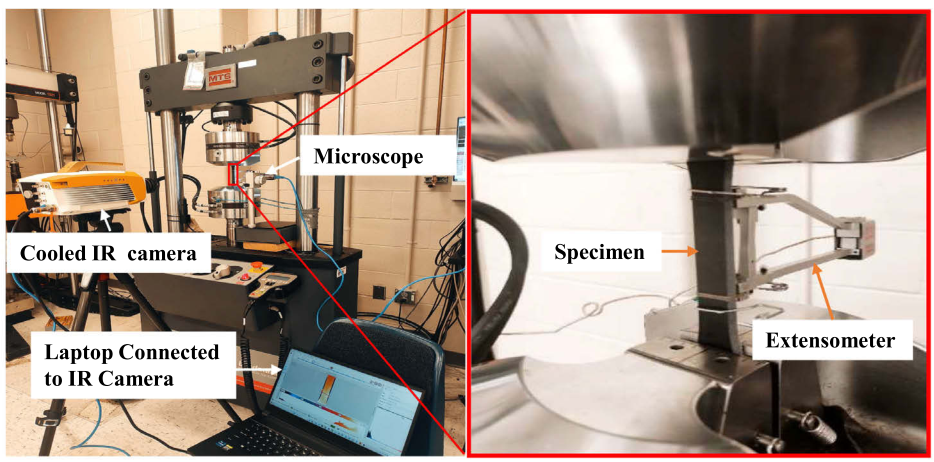

Fig. 4. Experimental set-up of in-situ surface temperature measurements using a cooled IR camera connected to a laptop with Reveal IR software using a UTM system with 5 cm gage length extensometer.

2.3. Quasi-static testing

All tests, static and fatigue, were performed using an MTS Landmark servohydraulic universal test frame (Model 370.25) with a capacity of 100 kN, as depicted in Fig. 4. Quasi-static tensile tests were conducted at a 2 mm/min displacement controlled loading to determine the mechanical properties – stiffness and ultimate tensile strength – of the CF/ABS composite plates. Specimen strains were monitored using an extensometer with a 5 cm gage length. A total of 5 specimens were tested to determine an average tensile strength (σ_{uts}) of 64.52 ± 2.17 MPa, failure strains (ϵ_f) of 0.82% ± 0.01%, and elastic modulus (E_0) 8.32 ± 0.02 GPa. This dataset served as the baseline for conducting fatigue testing. Furthermore, the tensile data indicated the uniformity of FOD/FLD along the bead direction of the CF/ABS laminates.

2.4. Fatigue testing using IRT

Tension–tension fatigue was conducted with a stress ratio $R = 0.1$ under sinusoidal load-controlled mode with values of maximum and minimum loads determined as percentages of the average σ_{uts} obtained from quasi-static tensile testing. Loading frequency for cyclic tests was maintained at 15 Hz. Gage pressure was consistently maintained at approximately 200 psi to avoid specimen slippage during the tests. A Telops Spark M150 medium wave infrared (MWIR) camera equipped with an InSb cooled detector, a 640 × 512-pixel resolution sensor, a 50 mm lens with a noise equivalent temperature difference (NETD) of 20 mK, and a spectral range spanning 3–5.4 μm was used for all the in-situ temperature measurements during fatigue testing. The thermal images were captured at an acquisition frequency of 100 Hz to enable the capture of multiple temperature signals during each load cycle. These temporal full-field temperature plots were used for harmonic analysis that yielded information about anelastic dissipative effects as described in Eq. (1) [66]. During these analyses, the region of interest (ROI) was restricted to a specific area measuring approximately 13 mm × 13 mm, centered around the specimen failure zone. All collected thermographic data was extracted using Reveal IR's software and processed in Matlab.

Fig. 5 shows a staircase cyclic loading at a constant stress ratio $R = 0.1$ with a loading frequency of 15 Hz, similar to the approach outlined in [36,37,42,67]. As described in later sections, HCFS is determined by plotting the ΔT_{stab} obtained for each step (σ_{max}). The HCFS denotes the point of intersection for the bi-linear curves that best fit the ΔT_{stab} versus σ_{max} data. This intersection point is found by observing the changing slopes of the ΔT_{stab} vs. σ_{max} curve. The step level of σ_{max} that shows the most significant change in slope indicates the inflection point, which identifies the HCFS of the test specimen. Identifying this intersection point requires determining the step rise (increment) and step size (number of cycles at each step level) of the step. The step size (N_{step}) was kept constant at 7500 cycles based on trial tests conducted to determine the phase II stabilized steady-state zone at every load level (see Fig. 1(a)). To ensure repeatability of test data, a minimum of three replicates were tested. The fatigue testing was stopped at the end of each load step, and the specimen was allowed to cool down to room temperature before the next load step. This cool-down phase is called the 'rest period' in Fig. 5. To maintain uniform material testing outcomes, the specimen must start each loading step at ambient room temperature. This requires adjusting rest periods between load levels to allow sufficient time for the specimen to cool down to ambient temperature after the previous load application. Following each rest

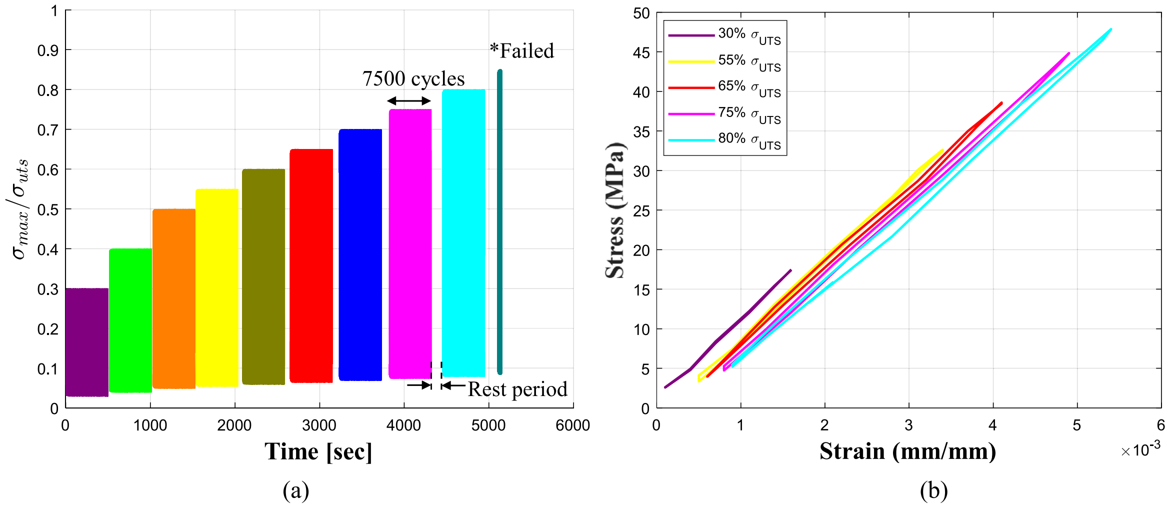

Fig. 5. Staircase loading applied to a specimen to determine HCFS rapidly: (a) Early increments of 10% σ_{uts} followed by 5% σ_{uts} increments to σ_{max} were used to determine HCFS. The stress ratio R = 0.1 was maintained throughout the test. The rest period between load steps ensured the specimen cooled down to room temperature after every step load, (b) Hysteresis energy for given load level @ N = 5000 cycle.

period in the staircase loading approach, a static test was performed to estimate stiffness degradation as a function of applied load cycles.

In addition to the IRT step-loading approach, traditional SN curves were developed for the CF/ABS specimens. Constant amplitude fatigue tests at 70%, 65%, 60%, 55%, 50%, and 35% σ_{uts} were performed at 5 Hz for $R = 0.1$, ensuring no perceptible increase in surface temperatures in compliance with the ASTM D638 standard [60]. Three replicates were tested for each load level. Specimens that did not fail till 3×10^6 cycles were considered as run-out consistent with literature [23, 25,48].

3. Results and discussion

3.1. Cyclic temperature stabilization and stiffness degradation

Fig. 6 depicts a representative in-situ temporal full-field temperature evolution for a 20% CF/ABS specimen undergoing accelerated fatigue testing using a staircase loading (cf. Fig. 5). Each thermogram depicts the stabilized phase II temperature for the applied load level described in Fig. 5 earlier. Based on these thermograms, the region indicating the maximum temperature within the gage section has been determined. This maximum temperature evolution within the gage section has been plotted in Fig. 7(a) for each applied step. It should be noted that Fig. 7(a) captures the 'rest period' shown in Fig. 5 with the temperatures for each step load starting from ambient room temperature. At higher applied load levels, the distinctive phase II stabilized plateau is missing, indicative of a rapid irreversible damage growth. Finally, the specimen was found to fail at 85% σ_{uts} maximum stress. The maximum temperature spatial location (cf. Fig. 6) coincides with the final failure location in the specimen.

An extensometer was used throughout the fatigue testing to correlate the temporal surface temperature evolution due to self-heating under fatigue loading with the corresponding volumetric stiffness degradation. It is worth noting that the extensometer provides a pathway for heat dissipation via conduction. However, the maximum mean temperatures coincide with the location of damage incipience and eventual final failure. Fig. 7(b) depicts the stiffness degradation of the test specimen under step loading. The stiffness degradation represents a characteristic progressive damage behavior wherein the damage magnitude gradually increases before final failure (approximately 12% in this case) [37]. Fig. 7(d) illustrates the temporal temperature and stiffness data for two different levels of applied CAF, namely 35% σ_{uts} and 65% σ_{uts}. The data is plotted against the normalized life N/N_f of the specimen, where N_f represents the failure life for the respective applied CAF. For 35% σ_{uts} CAF, N_f was chosen to be 3×10^6 cycles, the maximum number corresponding to a run-out test. Surface temperatures were recorded for the duration of the CAF tests. The two load levels have been selected to depict the damage and temperature correlation for two load cases, one below and the other above the fatigue limit. It is observed, the two parameters are closely correlated, similar to the results presented in [48]. Nevertheless, it is acknowledged that while surface temperature is a viable measure of fatigue, specific heat dissipation per unit volume could offer a more accurate indicator, given that surface temperatures are typically dependent on loading frequency and specimen geometry. Notably, defects in the AM-CM composites often lead to the formation of hot spots. In the current examination of phenomenological models, the findings from pristine specimens have been compiled for analysis supported by the uniform temperature over the gage section, as seen in Fig. 6.

A note about the damage mechanisms in SFTs: fiber–matrix interfacial friction followed by debonding has been recognized as the most dominant failure mode in the chosen SFTs, as corroborated by others [5,68,69]. Theoretically, the fiber ends of a chopped short fiber have a very high-stress concentration factor; these fiber ends act as heat sources upon cyclic load application. With increasing load cycles, debonding of the fiber–matrix interface progresses, with damage incipience occurring at the fiber ends. This debonding mode progresses with time in a stable fashion, represented by phase II of the temperature evolution curve at each load step. Eventually, a significant number of fiber–matrix debonds are triggered, leading to final failure accompanied by a surge in temperature (phase III). Scanning electron microscopy (SEM) conducted on the failed surfaces confirms that fiber–matrix debonding is the predominant damage mode, as elaborated in Section 3.6.

3.2. Fatigue limit comparison: IRT versus SN curve

The temperature evolution plots in Fig. 7(a) show how ΔT_{stab} changes as a function of σ_{max}. Up to an applied $\sigma_{max} = 50\%\sigma_{uts}$, the temperature remained uniform across the specimen surface (see Fig. 6). However, as the load level increases, a distinct 'hot zone' emerges, corresponding to the location of damage incipience in the specimen followed by eventual failure (Fig. 6). Notably, the temperature stabilizes over a brief range of cycles before failure. Fig. 8(b) illustrates the temperature increase plotted against the maximum applied stress, revealing a clear point where the dissipated heat increase is more

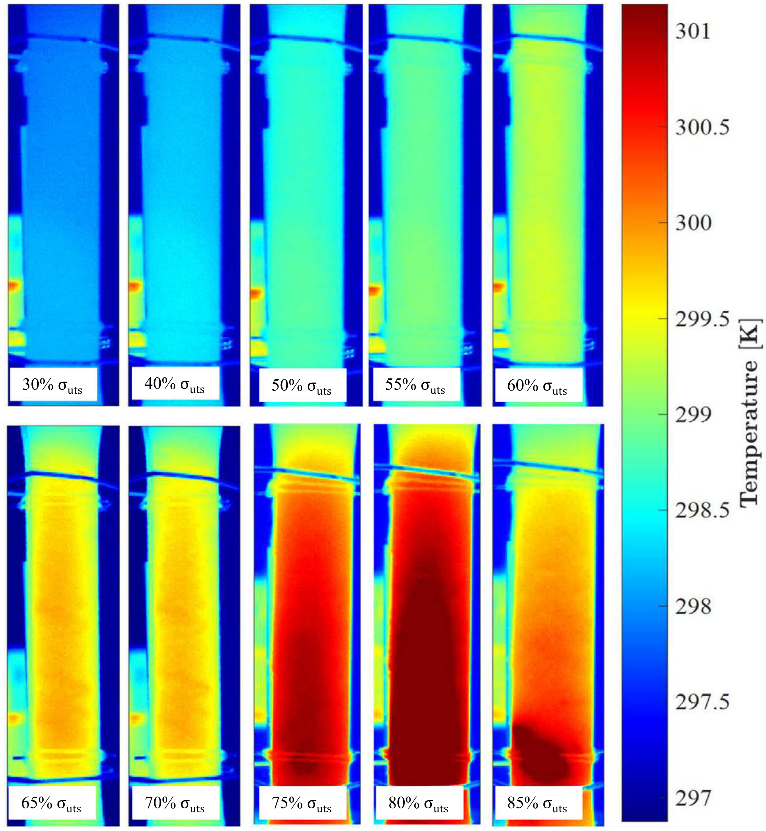

Fig. 6. Change in specimen surface temperature profile of a CF/ABS specimen with increasing loading cycles from the start of the experiment to failure. The corresponding applied load level is indicated in each sub-figure.

significant, representing an approximate fatigue limit of 54% σ_{uts}. In addition to IR fatigue testing, conventional SN curve results are shown in Fig. 8(a), yielding a fatigue limit of approximately 53% σ_{uts} for a 5 Hz frequency very close to that obtained from IRT. However, it should be noted that to obtain the SN curve for the 20% CB/ABS panels, *18 specimens were tested, three replicates at every load level, spanning over two weeks of testing*. On the other hand, the IRT fatigue testing was established using only*three specimens with a total test duration of 5 h*. Thus, the IRT approach provides an accelerated testing framework for rapidly estimating the fatigue limit.

3.3. Rate of heating and cooling index

The initial rate of heating (R_θ) and the rate of cooling (R_c) are barometers of the state of damage in a specimen, as discussed in Section 1. Methodically, the initial temperature rise is measured at the start of every new load step, and the tests are stopped after each loading cycle to measure the cooling rate. Fig. 9 depicts the estimation of fatigue limit using these measured R_θ and R_c, adopting the bi-linear approach described for ΔT_{stab} in Fig. 8(b). The analysis reveals a consistent trend: the material's temperature rate gradually rises at low-stress levels. However, as applied stress magnitude increases, the rate of damage development is also expected to increase, marked by increasingly pronounced temperature fluctuations. The cooling rate (R_c) also captures this effect. These results are particularly useful in designing experiments to assess the remaining life of a component. Since heating and cooling rates depend on the state of damage in a system, these indicators could potentially yield valuable information about the state of damage in a structure with an unknown load history [13,44]. The fatigue limits predicted by R_θ and R_c are relatively close, 56% σ_{uts} and 54% σ_{uts}, respectively. The R_θ and R_c values are found to diverge for load levels that cause significant damage within the load step; in this case, load levels beyond 70% σ_{uts}.

3.4. Second harmonic analysis (S_2)

As outlined in Eq. (1), harmonic analysis of temporal temperature data is a commonly employed method to discern the onset and progression of damage [25,38]. Specifically, the first harmonic signal (S_1) is associated with the thermoelastic stress analysis (TSA) effect, while the second harmonic term (S_2) captures the influence of dissipative mechanisms. The choice of a temperature data acquisition rate (100 Hz) and loading frequency (15 Hz) facilitated harmonic analysis of the thermal signals. Fig. 10 depicts the evolving S_2 signals in the vicinity of the final failure location, starting from 30% σ_{uts} till eventual failure at 85% σ_{uts}. Harmonic analysis of the temperature signals was conducted at each load level, ensuring the specimen had reached the steady-state phase II region.

A noteworthy observation is a steady increase in the radiometric temperature signal throughout each loading stage (see Fig. 11(a)). This trend is primarily influenced by the viscoelastic properties inherent in the matrix material [38]. A significant spike in the signal becomes apparent when damage mechanisms are initiated with S_2 exhibiting prominent variations when stress values exceed 55% σ_{uts}. The 98th percentile of S_2 over the chosen region of interest (ROI) is chosen for further analysis to exclude the influence of vibration or other effects that might influence the temperature signals. Residuals of the 98th percentile S_2 signal were evaluated following the approach recommended in [29], as shown in Fig. 11(b).

Analyzing the signal dynamics over individual sub-steps reveals a generally consistent trend: the 98th percentile S_2 residuals exhibit a threshold behavior, below 55% σ_{uts}, and no significant S_2 residual signals present. This indicates that the thermographic parameters are independent of the number of cycles for low-stress values. The identified threshold of 55% σ_{uts} represents the material's fatigue limit using the described harmonic analysis. Conversely, using S_{2max} versus σ_{max} plots overestimates the fatigue limit, yielding 58% σ_{uts}.

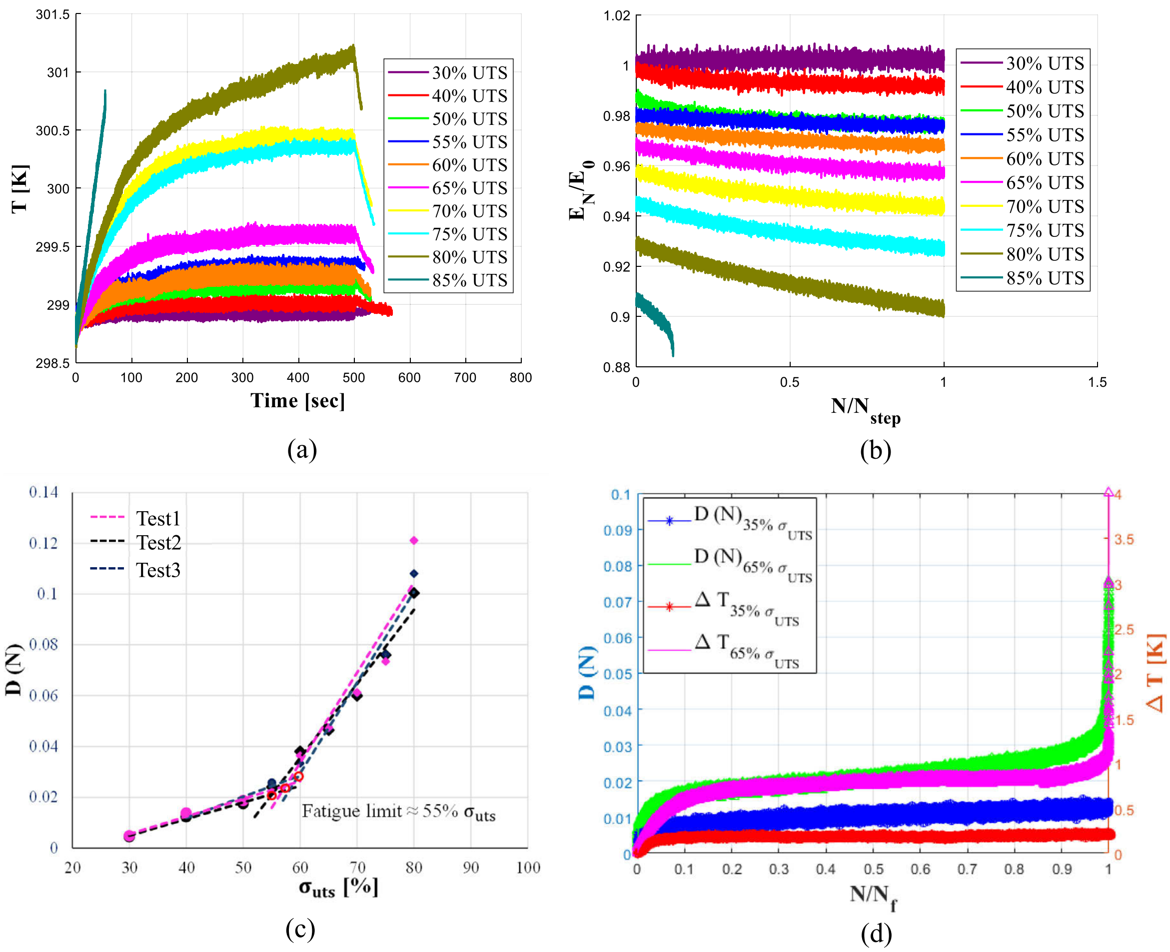

Fig. 7. (a) Maximum surface temperature evolution of a 20% CF/ABS specimen under step loading. The specimen was allowed to cool down after every load step. (b) Stiffness degradation was measured using an extensometer for the specimen under step loading, (c) Damage evolution under step loading showing a bi-linear behavior similar to ΔT_{stab}, and (d) Damage and change in temperature correlation for CAF 35% σ_{uts} and CAF 65% σ_{uts} at 5 Hz.

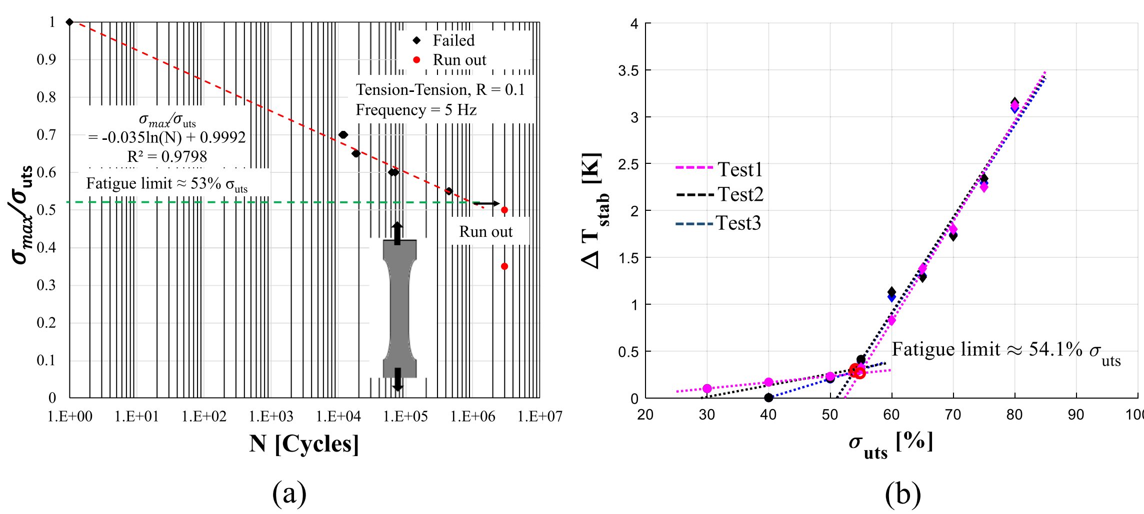

Fig. 8. (a) S-N curve-based estimation of the fatigue limit at 5 Hz. (b) Bi-linear approach to get fatigue limit using temperature change at 15 Hz frequency.

3.5. Comparative analysis of IRT methods with stiffness degradation

As discussed in Section 1, to rely on IRT-based fatigue limit characterization, a correlation between the measured surface temperatures and volumetric stiffness degradation, or damage, needs to be established. Fig. 12 illustrates damage ($D(N)$) correlation with the derived fatigue limits for the chosen staircase loading at 15 Hz frequency, considering ΔT_{stab}, S_{2max}, R_θ, and R_c. All IRT methods yield consistent estimates of the fatigue limit and exhibit a certain degree of scatter while comparing well with volumetric stiffness degradation (Table 1). The close fatigue limit values obtained using ΔT_{stab}, R_θ, and R_c can be attributed to their dependence on temperature change and energy

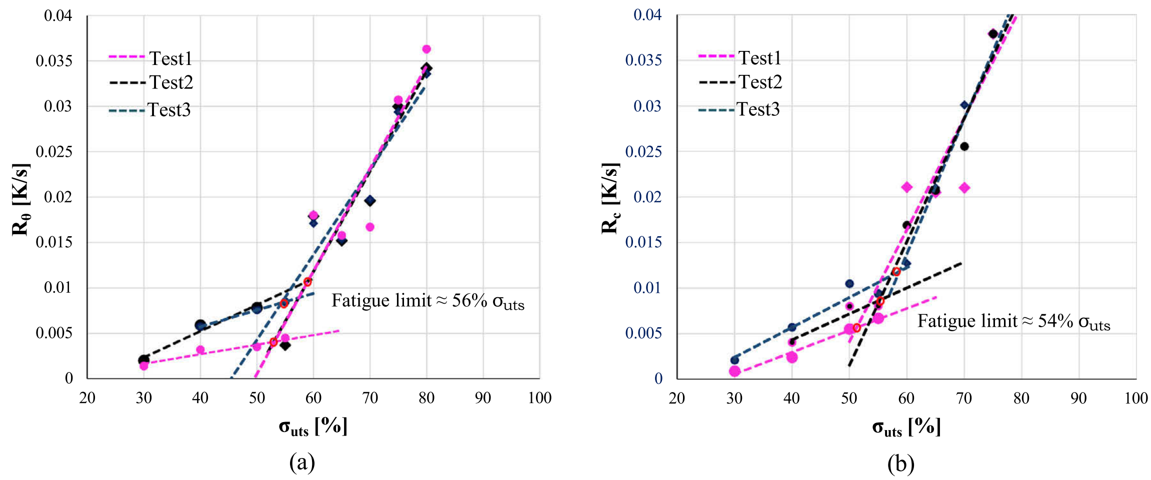

Fig. 9. Bilinear approach to get fatigue limit using: (a) R_0 approach, (b) R_c approach.

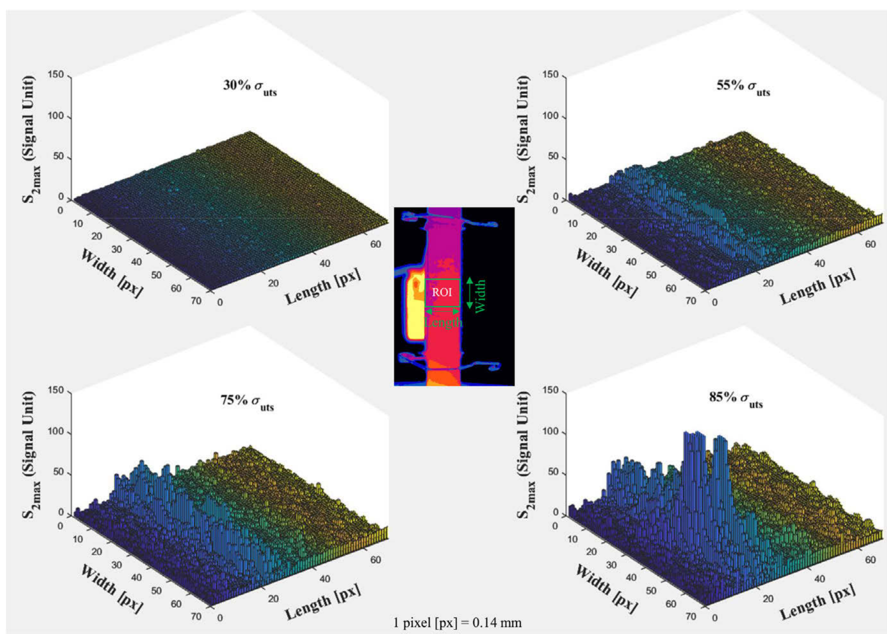

Fig. 10. Surface map of thermographic signal at S_2.

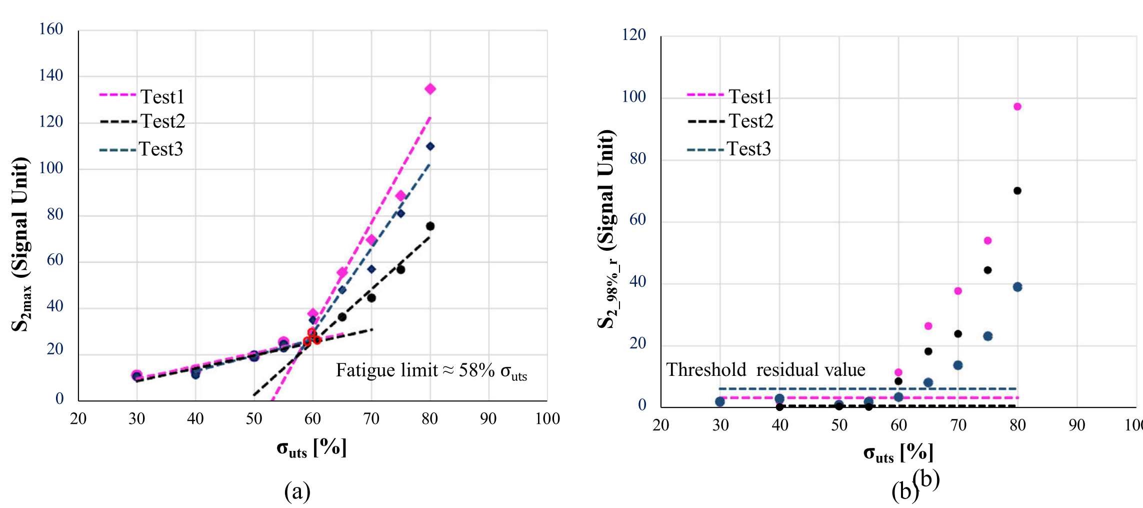

Fig. 11. Estimation of the fatigue limit with S_2 (a) Bi-linear approach to find fatigue endurance using S_2 limit, and (b) Residual of S_2.

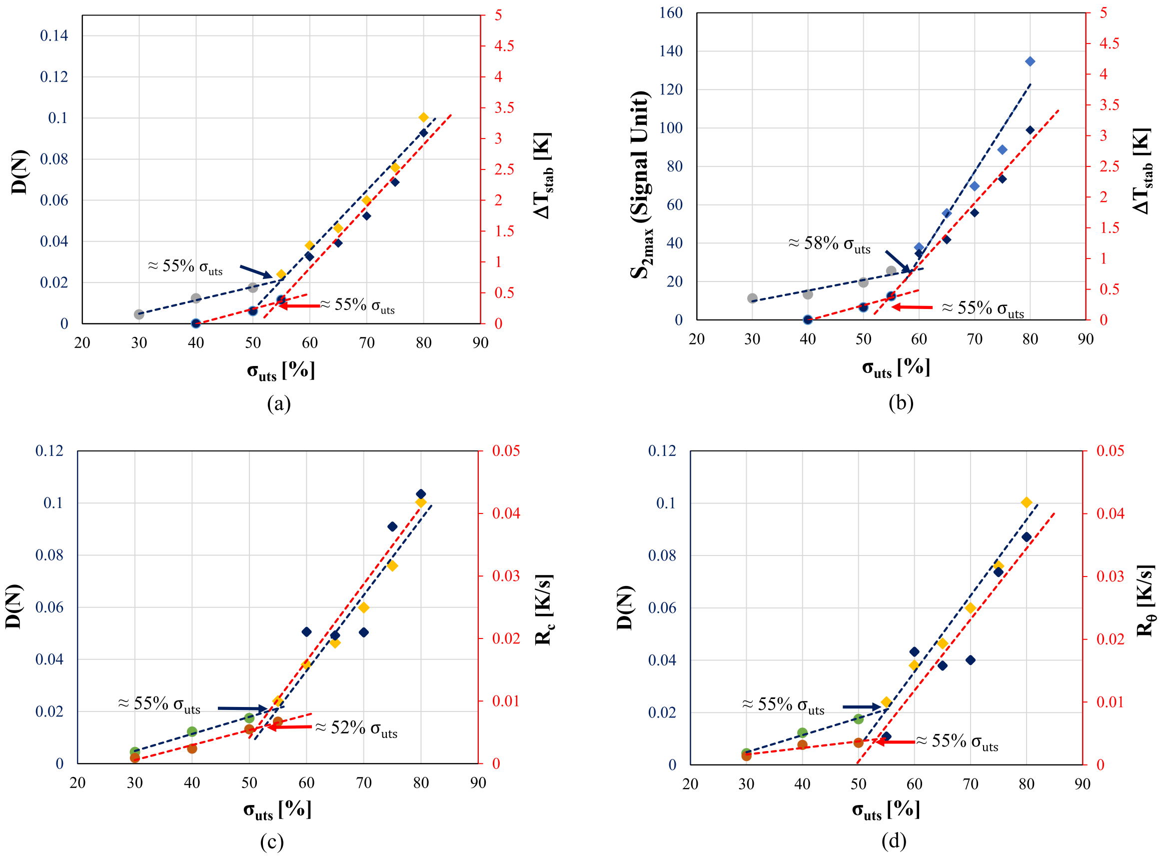

Fig. 12. Comparison of all IRT approaches (a) Damage accumulation over ΔT_{stab}, (b) S_{2max} over ΔT_{stab}, (c) Damage accumulation over R_c, (d) Damage accumulation over R_θ.

Table 1
Summary of comparison of all IRT approaches.

Sample number	ΔT_{stab}	$D(N)$	R_θ	R_c	$S_{2\max}$
1	54.92%	54.40%	54.90%	51.70%	58.10%
2	53.50%	55.00%	55.10%	53.80%	59.30%
3	54.10%	58.30%	58.00%	58.10%	57.80%
Average (% σ_{UTS})	54.10% ± 0.78%	55.56% ± 2.25%	56.05% ± 1.73%	54.47% ± 3.24%	58.41% ± 0.79%

dissipation, which also aligns with the close fatigue limit value obtained by the $D(N)$ method. On the other hand, S_{2max} demonstrates higher sensitivity to thermomechanical coupling and microstructural changes, such as matrix cracking or fiber realignment. These changes may not be as pronounced in the early stages, resulting in a higher fatigue limit obtained using this method than others. An average fatigue limit of approximately 54% σ_{uts} was found across all IRT methods, demonstrating their reliability and robustness.

The main advantage of using the IRT approach is that these measurement techniques provide accurate information about the incipient location of a looming damage before a significant damage event occurs. Fig. 13 depicts IR thermograms for two CF/ABS specimens, one pristine and the other with an initial process defect. For the pristine specimen (Fig. 13), fatigue damage initiation and final failure were found to occur within the grip region. For the specimen with the initial process defect, a hot spot occurs within a few hundred load cycles that later becomes the site for damage initiation and eventual final failure. The specimen with the initial defect fails at much lower load cycles than the pristine specimen. This phenomenon of process defects acting as regions of fatigue damage incipience is prescient for AM composites, requiring the careful characterization of process defects' effect on a structure's fatigue life [58,70]. The use of IRT as a means of rapid fatigue life estimation is expected to become valuable for rapidly correlating process defects with fatigue limits for AM composites. The results presented in this work would form the basis for future studies with process defects.

3.6. Failure analysis and fractography of AM-CM specimens

Fig. 14 depicts an SEM image of a failed 20% CF/ABS specimen used in the current work. As discussed earlier, in SFTs, the fiber ends exhibit the highest stress concentration regions acting as damage initiation regions. The primary damage mode in SFTs is fiber/matrix debonding, confirmed in the current fractographic investigation (see Fig. 14). Further observations across the sample's thickness revealed fiber pull-out and fiber breakage, distinctly highlighted in Fig. 14. The interphase between constituent materials significantly influences the eventual properties of composite structures. During the fractographic investigation, evidence of matrix porosity was discovered. However, it is important to note that the specimen exhibited a generally uniform and compact structure with minimal voids and pores, as explained in Section 2.2.

4. Conclusions and future work

A comparison of existing phenomenological approaches to rapid fatigue characterization of AM-CM chopped CF/ABS composite materials

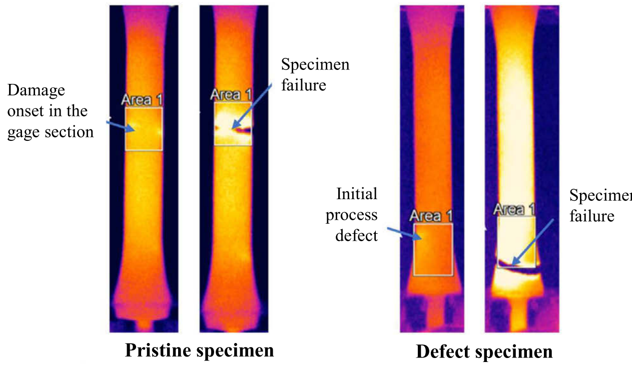

Fig. 13. Thermograms indicating the effect of process defects on fatigue damage onset and final failure in 20% CF/ABS AM-CM SFTs.

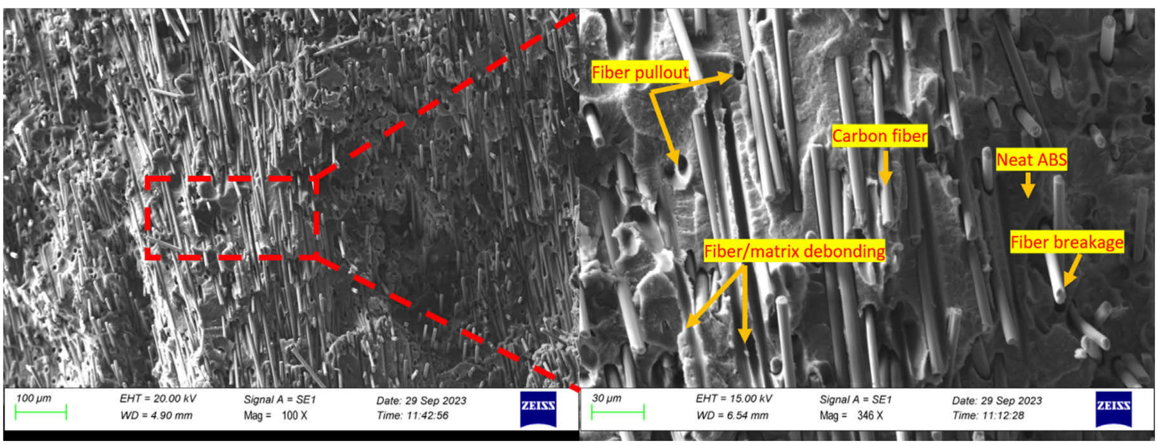

Fig. 14. Fractography showing fiber breakage.

using infrared thermography has been conducted in this work. Temporal surface temperatures measured during cyclic testing of CF/ABS systems have been analyzed using nontraditional IRT methods and compared with volumetric damage evolution to gain deeper insights into the interplay between material properties, temperature changes, and stiffness degradation. The following key findings emerge from this research:

1. Comparison of traditional SN-curve based fatigue limit with IRT approaches - ΔT_{stab}, S_{2max}, R_θ, and R_c - reveals a reasonably good match. A significant speed-up in testing time and the required number of specimens for determining the fatigue limit has been demonstrated. Thus, the IRT approaches can be used as an alternative to the more time-consuming SN approach for rapid quantification of fatigue limit, especially for AM composites, to establish process–structure–property relations.
2. The analysis introduces nontraditional fatigue assessment methods, such as the cyclic temperature stabilization method, rate of temperature change, double frequency signal (S_2), and damage accumulation method. These methods offer complementary insights into fatigue behavior, providing a more detailed understanding of material response and damage accumulation than traditional SN curve approaches.
3. Preliminary results indicate the promise of IRT methods for rapid process defect classification in AM composites under fatigue.
4. Furthermore, the fractography analysis offers valuable insights into the fracture behavior of CF/ABS composite materials, shedding light on interphase cohesion, the response of carbon fibers within the composite, and its orientation.

In summary, IRT-based fatigue characterization has been proven to be a promising means of assessing process–structure–property relations in AM composites. Future investigations will focus on understanding process defects' effect on AM composites' fatigue life via infrared thermography.

CRediT authorship contribution statement

P. Pathak: Conceptualization, Investigation, Methodology, Software, Data curation, Validation, Writing – original draft. **S. Gururaja:** Conceptualization, Investigation, Supervision, Funding acquisition, Writing – review & editing. **V. Kumar:** Funding acquisition, Investigation, Writing – review & editing. **D. Nuttall:** Investigation, Writing – review & editing. **A. Mahmoudi:** Methodology, Investigation, Writing – review & editing. **M.M. Khonsari:** Methodology, Writing – review & editing. **U. Vaidya:** Writing – review & editing.

Declaration of competing interest

The authors declare that they have no known competing financial interests or personal relationships that could have appeared to influence the work reported in this paper.

Data availability

No data was used for the research described in the article.

Acknowledgments

The research is partly supported by the US Department of Energy (DOE), Office of Energy Efficiency and Renewable Energy, Advanced Manufacturing Office, under contract DE-AC05-00OR22725 with UT-Battelle LLC. A.M. and M. K. acknowledge the support US National Science Foundation, grant number 2243755. The authors acknowledge Mr. Nithinkumar Manoharan, a graduate student of the Department of Aerospace Engineering, Auburn University, for his support during specimen fabrication and initial fatigue testing. A part of the paper was presented at the 2023 SEM Annual Conference held in Orlando, FL, USA, in June 2023.

References

[1] Brasington A, Sacco C, Halbritter J, Wehbe R, Harik R. Automated fiber placement: A review of history, current technologies, and future paths forward. Composites C 2021;6:100182.
[2] Coolest 3D printed cars. 2023, [Online]. Available: https://all3dp.com/2/coolest-3d-printed-cars [Accessed 06 January 2023].
[3] Composites world. 2023, [Online]. Available: https://www.compositesworld.com/articles/additive-manufacturing-adds-versatility-to-large-marine-structures- [Accessed 06 January 2023].
[4] Doddamani M, Bharath HS, Prabhakar P, Gururaja S. Material systems and methods. In: 3D printing of composites. Springer; 2023, p. 23–8.
[5] Huang HB, Huang ZM, Wan YP. Micromechanical predictions on elastic moduli of a short fiber composite with arbitrary geometric combination. Composites A 2023;168:107477.
[6] Seta B, Sandberg M, Brander M, Mollah MT, Pokkalla D, Kumar V, Spangenberg J. Modeling fiber orientation and strand shape morphology in three-dimensional material extrusion additive manufacturing. Composites B 2023;266:110957.
[7] Kim T, Trangkanukulkij R, Kim WS. Nozzle shape guided filler orientation in 3D printed photo-curable nanocomposites. Sci Rep 2018;8.
[8] AM-CM - Research & development world. 2023, [Online]. Available: https://www.rdworldonline.com/rd-100-2023-winner/am-cm [Accessed 06 January 2023].
[9] Awards - CAMX – The composites and advanced materials expo. 2023, [Online]. Available: https://www.thecamx.org/awards [Accessed 04 October 2023].
[10] Kumar V, Alwekar SP, Kunc V, Cakmak E, Kishore V, Smith T, Lindahl J, Vaidya U, Blue C, Theodore M, Kim S, Hassen AA. High-performance molded composites using additively manufactured preforms with controlled fiber and pore morphology. Addit Manuf 2021;37:101733.
[11] Van de Werken N, Tekinalp H, Khanbolouki P, Ozcan S, Williams A, Tehrani M. Additively manufactured carbon fiber-reinforced composites: State of the art and perspective. Addit Manuf 2020;31.
[12] Talreja R. 4 - Manufacturing defects in composites and their effects on performance. In: Irving P, Soutis C, editors. Polymer composites in the aerospace industry (second edition). 2nd ed.. 2020, p. 83–97.
[13] Meneghetti G. Analysis of the fatigue strength of a stainless steel based on the energy dissipation. Int J Fatigue 2007;29(1):81–94.
[14] Mohammadi B, Shokrieh MM, Jamali M, Mahmoudi A, Fazlali B. Damage-entropy model for fatigue life evaluation of off-axis unidirectional composites. Compos Struct 2021;270:114100.
[15] Jirandehi AP, Khonsari MM. Microstructure-sensitive estimation of fatigue life using cyclic thermodynamic entropy as an index for metals. Theor Appl Fract Mech 2021;112:102854.
[16] Khonsari M, Amiri M. Introduction to thermodynamics of mechanical fatigue. CRC Press; 2013.
[17] Jia Z, Pastor ML, Garnier C, Gong X. Fatigue life determination based on infrared thermographic data for MultiDirectional (MD) CFRP composite laminates. Compos Struct 2023;319:117202.
[18] Vassilopoulos A. The history of fiber-reinforced polymer composite laminate fatigue. Int J Fatigue 2020;134:105512.
[19] Talreja R. Fatigue damage in the presence of defects. In: Failure analysis of composite materials with manufacturing defects. 1st ed.. CRC Press; 2024, p. 102–31.
[20] McNally D. Short fiber orientation and its effects on the properties of thermoplastic composite materials. Polym-Plast Technol Eng 1977;8(2):101–54.
[21] Guo R, Li C, Niu Y, Xian G. The fatigue performances of carbon fiber reinforced polymer composites - A review. J Mater Res Technol 2022;21:4773–89.
[22] Kagawa H, Umezu Y, Sakaue K, Koyanagi J. Numerical simulation for the tensile failure of randomly oriented short fiber reinforced plastics based on a viscoelastic entropy damage criterion. Composites C 2023;10.
[23] Kalyanasundaram D, Gururaja S, Prabhune P, Singh D. Open hole fatigue testing of laser machined MD-CFRPs. Composites A 2018;111:33–41.
[24] Jia Z, Pastor ML, Garnier C, Gong X. A new method for determination of fatigue limit of composite laminates based on thermographic data. Int J Fatigue 2023;168:107445.
[25] Palumbo D, De Finis R, Demelio PG, Galietti U. A new rapid thermographic method to assess the fatigue limit in GFRP composites. Composites B 2016;103:60–7.
[26] Colombo C, Tridello A, Pagnoncelli AP, Biffi CA, Fiochhi J, Tuissi A, Vergani LM, Paolino DS. Efficient experimental methods for rapid fatigue life estimation of additive manufactured elements. Int J Fatigue 2023;167.
[27] Mahmoudi A, Khonsari MM. Evaluation of fatigue in unidirectional and cross-ply laminated composites using a coupled entropy-kinetic concept. J Compos Mater 2022;56(15):2443–54.
[28] Pitarresi G, Patterson EA. A review of the general theory of thermoelastic stress analysis. J Strain Anal Eng Des 2003;38:405–17.
[29] Palumbo D, Galietti U. Data correction for thermoelastic stress analysis on titanium components. Exp Mech 2016;56(3):451–62.
[30] Quinlan A, Castro O, Dulieu-Barton JM. Towards assessment of fatigue damage in composite laminates using thermoelastic stress analysis. Composites C 2023;12:100377.
[31] Leveuf L, Marco Y, Saux VL, Olhagaray J, Leclercq S, Navratil L. Fast screening of the fatigue properties of thermoplastics reinforced with short carbon fibers based on thermal measurements. Polym Test 2018;68.
[32] Reifsnider KL, Williams RS. Determination of fatigue-related heat emission in composite materials. Exp Mech 1974;14(12):479–85.
[33] Roylance D. Engineering viscoelasticity. Eng J 2001;2139.
[34] Naderi M, Amiri M, Khonsari MM. On the thermodynamic entropy of fatigue fracture. Proc R Soc A 2010;466(2114):423–38.
[35] Kahirdeh A, Naderi M, Khonsari MM. On the role of cooling on fatigue failure of a woven glass/epoxy laminate. J Compos Mater 2013;47(15):1803–16.
[36] Fargione G, Geraci A, Rosa GL, Risitano A. Rapid determination of the fatigue curve by the thermographic method. Int J Fatigue 2002;24(1):11–9.
[37] Montesano J, Fawaz Z, Bougherara H. Use of infrared thermography to investigate the fatigue behavior of a carbon fiber reinforced polymer composite. Compos Struct 2013;97:76–83.
[38] Rosa GL, Risitano A. Thermographic methodology for rapid determination of the fatigue limit of materials and mechanical components. Int J Fatigue 2000.
[39] Huang J, Pastor ML, Garnier C, Gong X. Rapid evaluation of fatigue limit on thermographic data analysis. Int J Fatigue 2017;104:293–301.
[40] Guo FL, Hu JM, Guan T, Fu YT, Huang CY, Li YQ, Fu SY. Modeling and characterizations of mechanical behaviors of short carbon fiber and short glass fiber reinforced polyetherimide composites. Compos Sci Technol 2022;229:109685.
[41] Colombo C, Trunal B, Flavia L, Laura V. Effect of delamination on the fatigue life of GFRP: A thermographic and numerical study. Compos Struct 2019;218:152–61.
[42] Pothnis JR, Hajagolkar AK, Anilchandra AR, Das R, Gururaja S. Open-hole fatigue testing of UD-GFRP composite laminates containing aligned CNTs using infrared thermography. Compos Struct 2023;324:117557.
[43] Mahmoudi A, Khonsari M. Entropic characterization of fatigue in composite materials. In: Encyclopedia of materials: Plastics and polymers. 2022.
[44] Amooie MA, Khonsari MM. On the effect of environmental temperature on fracture fatigue entropy. Int J Fatigue 2023;168:107411.
[45] Ali M, Bijan M. Theoretical-experimental investigation of temperature evolution in laminated composites due to fatigue loading. Compos Struct 2019;225.
[46] Haghshenas A, Jang JY, Khonsari MM. On the intrinsic dissipation and fracture fatigue entropy of metals. Mech Mater 2021;155:103734.
[47] Kordatos EZ, Dassios KG, Aggelis DG, Matikas TE. Rapid evaluation of the fatigue limit in composites using infrared lock-in thermography and acoustic emission. Mech Res Commun 2013;54:14–20.
[48] Sourd X, Zitoune R, Crouzeix L, Coulaud M, Lamouche D. Influence of the damage generated by abrasive water jet texturing on the tensile static and fatigue behaviour of 3D woven composite in the context of repair. Composites A 2021;149:106567.
[49] Laiarinandrasana L, Morgeneyer TF, Cheng Y, Helfen L, Le Saux V, Marco Y. Microstructural observations supporting thermography measurements for short glass fibre thermoplastic composites under fatigue loading. Contin Mech Thermodyn 2020;32(2):451–69.
[50] Feng Y, Gao C, He Y, An T, Fan C, Zhang H. Investigation on tension tension fatigue performances and reliability fatigue life of T700/MTM46 composite laminates. Compos Struct 2016;136:64–74.
[51] Derusova DA, Vavilov VP, Shpilnoi V, Siddiqui AO, Prasad YLVD, Druzhinin NV, Zhvyrblya VY. Characterising hidden defects in GFRP/CFRP composites by using laser vibrometry and active IR thermography. Nondestruct Test Eval 2022;37(6):776–94.
[52] Daim S, Cunningham PR, Marshall S, Silva C. Open hole quasi-static and fatigue characterisation of 3D woven composites. Compos Struct 2015;131:765–74.
[53] Duchene P, Chaki S, Ayadi A, Krawczak P. A review of non-destructive techniques used for mechanical damage assessment in polymer composites. J Mater Sci 2018;53(11):7915–38.
[54] Degrieck J, Paepegem WV. Fatigue damage modeling of fiber-reinforced composite materials. Appl Mech Rev 2001;54(4):279–300.

[55] Alam P, Mamalis D, Robert C, Floreani C, Brádaig MO. The fatigue of carbon fiber reinforced plastics - A review. Composites B 2019;166:555–79.

[56] Shabani P, Taheri-Behrooz F, Samareh-Mousavi SS, Shokrieh MM. Very high cycle and gigacycle fatigue of fiber-reinforced composites: A review on experimental approaches and fatigue damage mechanisms. Prog Mater Sci 2021;118:100762.

[57] Quaresimin M, Susmel L, Talreja R. Fatigue behaviour and life assessment of composite laminates under multiaxial loadings. Int J Fatigue 2010;32(1):2–16.

[58] Chevalier PL, Kassapoglou C, Gürdal Z. Fatigue behavior of composite laminates with automated fiber placement induced defects- a review. Int J Fatigue 2020;140:105775.

[59] Jia Z, Pastor ML, Garnier C, Gong X. Fatigue life determination based on infrared thermographic data for multidirectional (MD) CFRP composite laminates. Compos Struct 2023;319:117202.

[60] D20 Committee. Standard test method for tensile properties of plastics. 2010, http://dx.doi.org/10.1520/D0638-10.

[61] Abderrafai Y, Mahdavi M, Sosa-Rey F, Herard C, Navas I, Piccirelli N, Levesque M, Therriault D. Additive manufacturing of short carbon fiber-reinforced polyamide composites by fused filament fabrication: Formulation, manufacturing and characterization. Mater Des 2022;214.

[62] Tekinalp H, Kunc V, Velez-Garcia G, Duty C, Love L, Naskar A, Blue C, Ozcan S. Highly oriented carbon fiber–polymer composites via additive manufacturing. Compos Sci Technol 2014;105.

[63] Alwekar S, Yeole P, Kumar V, Hassen A, Kunc V, Vaidya U. Melt extruded versus extrusion compression molded glass-polypropylene long fiber thermoplastic composites. Composites A 2021;144.

[64] Hmeidat N, Elkins D, Peter H, Kumar V, Compton B. High-performance molded composites using additively manufactured preforms with controlled fiber and pore morphology. Addit Manuf 2021;37.

[65] Hmeidat N, Elkins D, Peter H, Kumar V, Compton B. Processing and mechanical characterization of short carbon fiber-reinforced epoxy composites for material extrusion additive manufacturing. Composites B 2021;223.

[66] Liakat M, Khonsari M. On the anelasticity and fatigue fracture entropy in high-cycle metal fatigue. Mater Des 2015;82:18–27.

[67] Manoharan N, Pathak P, Gururaja S, Kumar V, Vaidya U. Rapid fatigue characterization via infrared thermography of AM-CM composites. In: Challenges in mechanics of biological systems and materials, thermomechanics and infrared imaging, time dependent materials and residual stress. vol. 2, Springer Nature Switzerland; 2023, p. 53–8.

[68] Raphael I, Saintier N, Rolland H, Robert G, Laiarinandrasana L. A mixed strain rate and energy based fatigue criterion for short fiber reinforced thermoplastics. Int J Fatigue 2019;127.

[69] Gandhi UN, Goris S, Osswald TA, Song YY. 4 - Microstructure in discontinuous fiber-reinforced composites. In: Discontinuous fiber-reinforced composites : Fundamentals and applications. Hanser ed.. 2020, p. 95–176.

[70] Quaresimin M, Carraro PA, Mikkelsen LP, Lucato N, Vivian L, Brøndsted P, Sørensen BF, Varna J, Talreja R. Damage evolution under cyclic multiaxial stress state: A comparative analysis between glass/epoxy laminates and tubes. Composites B 2014;61:282–90.